20XX-01-XXXX

Hydrogen Engine Insights: A Comprehensive Experimental Examination of Port Fuel Injection and Direct Injection

Mohamed Mohamed Brunel University London, Kevin Longo, Brunel University London, Hua Zhao Brunel University London, Jonathan Hall, Mahle Powertrain Ltd Anthony Harrington Mahle Powertrain Ltd

Abstract

The environmental and sustainable energy concerns in transport are being addressed through the decarbonisation path and the potential of hydrogen as a zero-carbon alternative fuel. Using hydrogen to replace fossil fuels in various internal combustion engines shows promise in enhancing efficiency and achieving carbon-neutral outcomes. This study presents an experimental investigation of hydrogen (H_2) combustion and engine performance in a boosted spark ignition (SI) engine. The H_2 engine incorporates both port fuel injection (PFI) and direct injection (DI) hydrogen fuel systems, capable of injecting hydrogen at pressures of up to 4000 kPa in the DI system and 1000 kPa in the PFI operations. This setup enables a direct comparison of the performance and emissions of the PFI and DI operations. The study involves varying the relative air-to-hydrogen ratio (λ) at different speeds to explore combustion and engine limits for categorising and optimising operational regions.

Furthermore, load sweep tests are conducted at various engine speeds to evaluate the advantages of the H_2 direct injection system over the PFI system and to analyse the characteristics of NOx emissions. Additionally, a matrix of inlet and exhaust valve timings is tested for each injection system to assess the valve timings and their interactions with injection setups on combustion, engine performance and emissions. The main findings of this study demonstrate that both PFI and DI hydrogen systems offer the benefit of zero carbon emissions and improved indicated thermal efficiency (ITE) when used in an engine designed and tuned for gasoline combustion. The DI hydrogen system, in particular, exhibits 2% higher ITE than PFI as well as producing higher power output. This enhancement can be attributed to the DI's ability to operate under stoichiometric conditions, thanks to higher injection pressure and late injection timing during the intake stroke. This configuration mitigates backfire occurrences and prevents hydrogen from bypassing through the exhaust, thus enhancing combustion efficiency.

1. Introduction

Conventional petroleum-based fuels such as gasoline and diesel are still a significant source of fuels in the transportation sector. Nevertheless, those fuels are associated with the considerable generation of pollutant emissions such as carbon monoxide (CO), hydrocarbons (HC) and nitrogen oxides (NOx). Moreover, hydrocarbon fuels also produce greenhouse gas (GHG), such as carbon dioxide (CO_2), which is considered a major factor for global warming and responsible for global climate change.

Therefore, regulatory authorities and governments have recently reviewed their carbon emission reduction targets. Stringent emission regulations for passenger and light commercial vehicles have been implemented worldwide in transportation. Evident examples are Executive Order 14037 [1] from the United States of America (USA), which is targeting to have 50% of new passenger cars and light-duty vehicles being zero emissions vehicles (ZEV) – zero CO_2 emissions – by 2030, or the Regulation (EU) 2023/851 [2] from European Union, which aims to have only the sale of ZEV from 2035. Thus, the need for lowering tailpipe emissions is pushing the development of new solutions.

Battery electric vehicles (BEV) have exponentially increased in the past decade, while fuel cell electric vehicles (FCEV) have emerged in the market in recent years. Nevertheless, BEVs are less desirable in some applications due to lower range-to-weight ratio, higher refuelling time and excessive costs. Also, the production process of batteries requires the use of rare and toxic raw materials and recycling problems, making their zero-emission status highly questionable [3]. Likewise, FCEVs are expensive compared to their internal combustion engine (ICE) counterparts due to new technology under development and the need for high hydrogen purity as well, and their durability is still lower than expected for both light-duty and heavy-duty sectors [4, 5, 6]. On the other hand, biofuels [7, 8] and alcohol-based fuels [9, 10], which are classified as low-carbon, are promising solutions in ICEs for a rapid reduction of carbon emissions for low-to-medium term applications. Nevertheless, they will not suit the aforementioned long-term ZEV regulations.

Another emerging option that has been investigated is the use of zero-carbon fuels, such as ammonia (NH_3) and hydrogen (H_2). These fuels do not contain carbon atoms in their chemical composition and, when produced from renewable sources, can ensure that no carbon is emitted throughout their entire life cycle [11, 12]. Hence, it is possible to significantly mitigate the generation of HC, CO, and CO_2 during the combustion process. However, a minor amount of these emissions may still be produced due to the partial burning of lubricating oil in the combustion chamber [13, 14].

Using H_2 in an ICE can bring several advantages in addition to eliminating the problem of carbon emissions. It can be readily implemented in ICEs with minor modifications, and its high-octane number (above 130) and high auto-ignition temperature lead to high resistance to end-gas autoignition combustion [15]. Furthermore, the burning rate of hydrogen is much higher than gasoline's, which enhances the combustion stability, while its high diffusion coefficient may promote a more homogeneous combination of air and fuel than gasoline [16]. The flammability of H_2 is much broader than

Cite as: Mohamed, M., Longo, K., Zhao, H., Hall, J. et al., "Hydrogen Engine Insights: A Comprehensive Experimental Examination of Port Fuel Injection and Direct Injection," SAE Technical Paper 2024-01-2611, 2024, https://doi.org/10.4271/2024-01-2611

conventional hydrocarbon fuels, allowing for much leaner operation without the need for higher ignition energy [17, 18]. One advantage of lean operation is a lower probability of abnormal combustion, such as backfire, pre-ignition and surface ignition. These issues are frequently noticed under stoichiometric conditions, which usually restrict the engine load and power output [17, 18, 19]. Another advantage of leaner operation is that the engine-out NOx drops significantly with relative air-fuel ratio (λ) values higher than 2 [20]. White et al. [21] reported that a boosted hydrogen ICE running at lean conditions can achieve very low NOx levels without any aftertreatment system. This is essential, as one of the main disadvantages of hydrogen combustion is the NOx generation due to its high flame temperature, which can lead to thermal dissociation and oxidation of nitrogen in atmospheric air during the combustion [22]. Therefore, a typical H_2 combustion strategy is running the engine at an ultra-lean mixture while achieving the desired power density and higher engine load. In order to achieve this strategy, a high level of intake-boosting air is then required [23]. However, leaner combustion can result in lower combustion efficiency (more unburned fuel), which consequently results in lower thermal efficiency as well as lower exhaust gas temperature (EGT), negatively impacting the enthalpy available for driving turbochargers [17].

Navale et al. [24] experimentally investigated the differences in performance, engine-out emissions and combustion characteristics of hydrogen and gasoline fuels in a naturally aspirated single-cylinder SI engine. The test results demonstrated that although a hydrogen engine's brake thermal efficiency (BTE) was 3% higher than gasoline, the maximum brake power for hydrogen was reduced by 19% compared to gasoline. Moreover, the problem of surface ignition and backfire occurred at the lower relative air-fuel ratios (rich operation). This means the power deficiency can be even higher if the engine runs at leaner conditions to avoid abnormal combustion. Intake-air pressure-boosting is an effective strategy for increasing engine power in conventional petroleum-fueled engines.

On the other hand, Nagalingam et al. [25] studied a single-cylinder hydrogen engine with boosting intake air up to 260 kPa. The results demonstrated that when compared to a naturally aspirated hydrogen engine, the power output increased by 233% at a speed of 1200 rpm. Berckmüller et al. [26] also reported a 0.5 L supercharged hydrogen engine with 185 kPa of intake air pressure, and it was found that indicated mean effective pressure (IMEP) could overtake 1800 kPa for all working conditions with variable compression ratios.

The injection mode also significantly affects airflow in the intake port, space-time distribution, and hydrogen development when it enters the cylinder, affecting the charge mixture and the combustion process [27]. The two most common approaches are port fuel injection (PFI), where the injector is located in the intake manifold, and direct injection (DI), where the injector can be central or side-located.

PFI is considered a more straightforward method to retrofit existing engines due to the easy installation of an injector in the intake port, without modifying the hardware, and with low injection pressure requirements. It also promotes a more homogenous mixture since the injection timing happens during the intake stroke, providing enough mixing time. However, this injection mechanism is often associated with reduced thermal efficiency and torque output as a consequence of the lower volumetric energy density of hydrogen. This is owing to the application of lower injection pressures. In addition, the risk of backfire is also a drawback of this injection system [28, 29]. Park et al. [30] replaced the fuel injector of the PFI gasoline engine with an H_2 injector and found that the larger volume ratio of hydrogen led to a low mixture intake volume, which resulted in lower torque output, while backfire problem to solve became more severe as speed increased.

By contrast, DI can prevent backfire in the intake manifold and minimise pre-ignition because fuel residence time in the cylinder can be shorter. Hence, the timing of the injection is also a crucial factor. The volumetric efficiency is significantly influenced by the injection pressure and injection time. Higher pressures and late injection, particularly during the later stage of the compression stroke, can lead to increased thermal efficiency and power output. This provides a notable advantage compared to the PFI system [28]. Mohammadi et al. [31] conducted a study comparing the effects of intake and compression stroke injections in a light-duty SI single-cylinder engine. The main conclusion reported was that direct injection of hydrogen effectively mitigates the occurrence of backfire. Nevertheless, it was discovered that increasing the quantity of hydrogen injected decreased the intake air volume and, therefore, the volumetric efficiency, leading to significant limitations on the maximum power output. On the other hand, the injection of hydrogen during the compression stroke tends to reduce knock and enhance both thermal efficiency and maximum output power. Injecting hydrogen during the later stage of the compression stroke can result in further improvement in thermal efficiency, reaching 38.9%. Additionally, under high engine output conditions, late hydrogen injection can greatly decrease the amount of NOx emissions because of the stratified operation. Despite this, the implementation of late injection requires the utilisation of injectors with high flow rates to facilitate the thorough mixing of hydrogen with the air prior to ignition timing. [26].

Another approach to mitigate hydrogen combustion limitations investigated in the past years is the variable valve timing. It can enable the hydrogen engine to run stoichiometric without backfiring through better scavenging exhaust gases [26]. Additionally, Verhelst et al. [29] investigated the effect of valve timing in a 1.8 L SI four-cylinder engine and concluded that varying the intake valve timing can slightly increase engine load at leaner conditions. As a result, BTE is significantly higher, reaching about 35% at λ 2.

It is evident that previous research has demonstrated that ICEs fueled by hydrogen can provide a valuable solution towards achieving net zero carbon targets. Although both PFI and DI can be adopted for an H_2 engine, there are limited results on the direct comparison between the two setups in the same engine in terms of their thermal efficiency across the entire engine load operation range at different speeds, the required amount of boosting level for load variation for different injection systems or optimising the H2 slip. As a result, the aim of this study carried out on a boosted light-duty SI single-cylinder engine, is to provide a better understanding of the impact of PFI and DI arrangements on the engine's performance and emissions under various engine speeds, engine loads, relative air-fuel ratios, and valve timings. Therefore, the experiments were divided into three main segments: λ sweep, engine load sweep, and cam envelope sweep.

2. Experimental setup

The experimental facility has been utilising liquid fuels for the past few years. However, significant modifications are required to transition to hydrogen as the primary fuel source and enable various operational techniques, such as hydrogen PFI and DI technologies. One of the primary obstacles hydrogen faced was determining the new risk assessment for the hydrogen supply line to ascertain the hydrogen source's location, given its capacity to store liquid fuel within the same test cell. In contrast to automobile and transportation applications, the operation of the test cell using hydrogen necessitates an isolated and

permanent site for safely storing the hydrogen bottles without imposing any potential hazards within the test cell. Consequently, the chosen solution involved securely isolating and adequately ventilating the bottles outside the test cell. This was achieved by locating them in a semi-enclosed space without a ceiling and surrounded by fire shields.

Additionally, it is advantageous to have all supply line accessories, such as pressure regulators, sensors, flow meters, and shutdown valves, located outside the test cell. This arrangement restricts the number of connections, considerably reducing the potential risk of leakage within the test cell.

The test cell has been outfitted with an additional ATEx extraction system featuring a flexible hood to maximise air ventilation. A Hydrogen sensor is installed in the air intake and linked to an automated shutdown Programmable Logic Controller (PLC) system. This system is designed to respond automatically by interrupting the supply line and purging the double pipe with nitrogen if the hydrogen level exceeds 3%. A thermal fuse was also installed in the intake manifold to activate the automated shutdown PLC when the intake temperature exceeds 130 °C in case of severe backfires during H2 PFI operations. This automated shutdown can also be triggered by another H2 sensor in the crankcase ventilation system to prevent the potential accumulation of hydrogen.

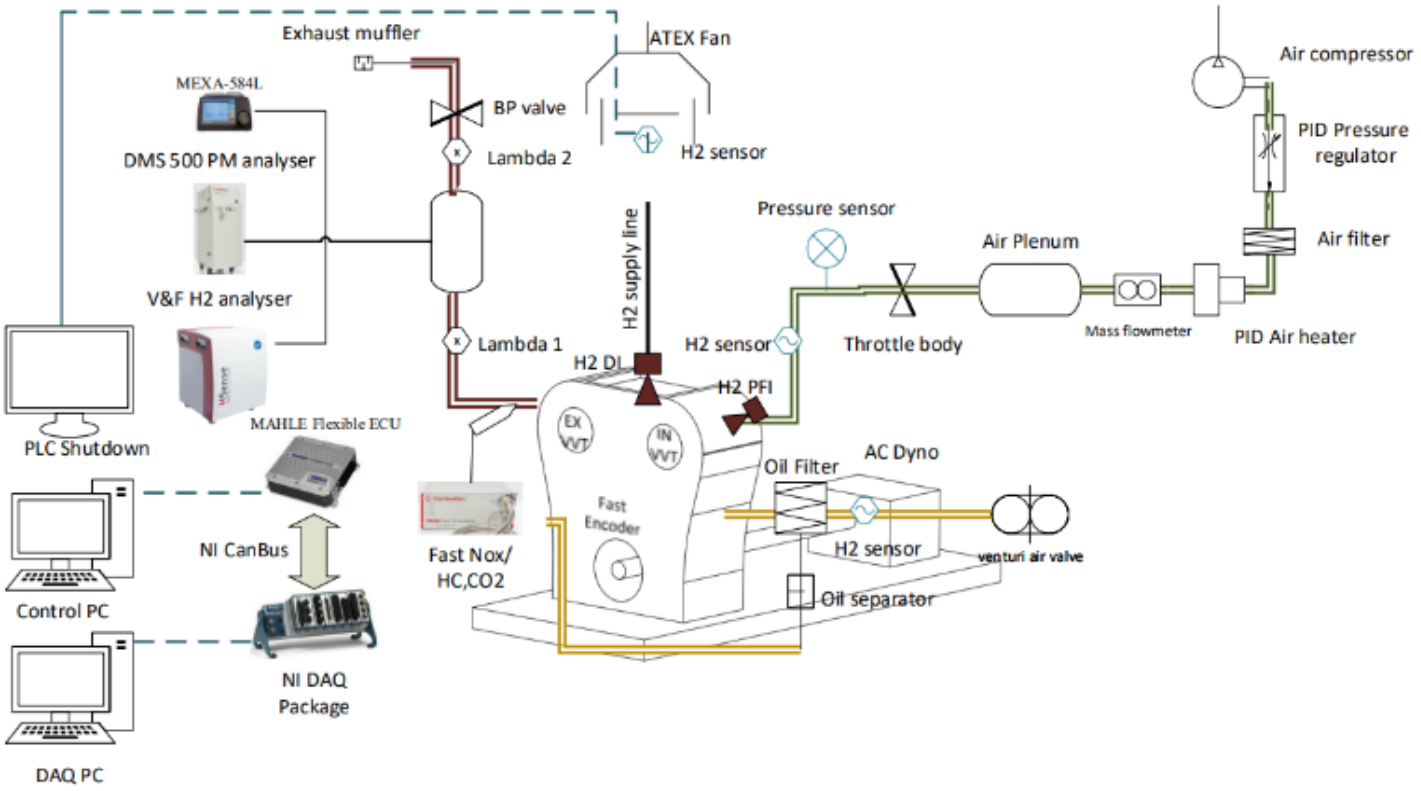

Figure 1: Schematic of H2IC test cell setup

2.1 Engine setup

Figure 1 depicts a schematic diagram of the SI single-cylinder engine provided by MAHLE Powertrain that was utilised to evaluate the performance and emissions of hydrogen in two different injection configurations: central direct injection and port fuel injection. The engine has a MAHLE adaptable electronic control unit (ECU), facilitating a seamless transition between PFI and DI engine operation. The engine utilised DI-CHG10 injectors manufactured by Phinia for direct and side-port fuel injection, enabling hydrogen injection ranging from 200 to 1000 kPa in the PFI system and 1000 to 4000 kPa in the DI system. A forced crankcase ventilation system was adopted to address potential hydrogen-related risks. Its output was sent to the extraction hood and monitored by a hydrogen sensor. If the hydrogen concentration exceeds 3%, the PLC system will automatically initiate a warning; then, at 4%, it cuts the hydrogen supply, as per Figure 1.

The engine incorporates fully variable valve timings for both the intake and exhaust cams, allowing flexibility in determining the optimal valve timing and overlap configuration for each injection system. Furthermore, the ECU enables the adjustment of the fuel injection timing and pressure, offering the ability to control the start or end of the injection process as needed. Furthermore, the engine has an external boosting system with a maximum boost pressure of 400 kPa. It also has an external air heater to regulate the intake temperature accurately. The main engine specs are in Table 1.

Table 1. Engine specifications

Configuration	Single Cylinder
Displaced volume	400 cc
Stroke x Bore	73.9 mm x 83 mm
Compression Ratio	11.3: 1
Number of Valves	4
Exhaust Valve Timing	EMOP (Exhaust Maximum Opening Point) 100-140 CAD BTDC, 11 mm Lift, 278 CAD Duration

Inlet Valve Timing	IMOP (Intake Maximum Opening Point) 80-120 CAD ATDC, 11 mm Lift, 240 CAD Duration
Injection System	Central Direct Injection outwardly opening spray ≤ 20000 kPa for gasoline and up to 4000 kPa for H_2 PFI injector up to 1000 kPa
Injection Control	MAHLE Flexible ECU (MFE)
Injection Control	Electronic coil-on-plug system with centrally mounted Spark plug

2.2 Fuel system and proprieties

The hydrogen supply system commences at the hydrogen bottles in an isolated space. The outlet is connected to a first-stage control panel. The hydrogen gas pressure is reduced and monitored by a pressure sensor. The hydrogen line is then connected to a solenoid valve before reaching the hydrogen flowmeter. Positioning the hydrogen flowmeter downstream of the initial stage is to mitigate any potential impact on the final pressure delivered to the injector resulting from pressure drops induced by the flowmeter. In the second stage control panel, another pressure regulator is employed to reduce the hydrogen pressure to the PFI or DI injection pressure. The second panel is equipped with an additional pressure sensor and a safety solenoid valve, which serve the purpose of isolating the line and minimising the quantity of H_2 in the pipe line in the event of hydrogen leakage.

In order to prevent any leaked hydrogn in the hydrogen pipe in the test cell from ententering the room, two double vacuum tubing systems were designed and installed for the PFI and DI hydrogen supply line between the fuel injector and the external hydrogen pipes. , addresses the issue of potential Hydrogen leakage in the pipeline. The double vacuum tube is connected to the pipeline, ensuring any leaked. A pressure sensor was installed to detect hydrogen leakage in the space between the inner hydrogen pipe and the outer pipe. In the case of hydrogen leakage detected, a nitrogen based purging system will be activated to remove the leaked hydrogen. This setup is visually depicted in the accompanying Figure 2.

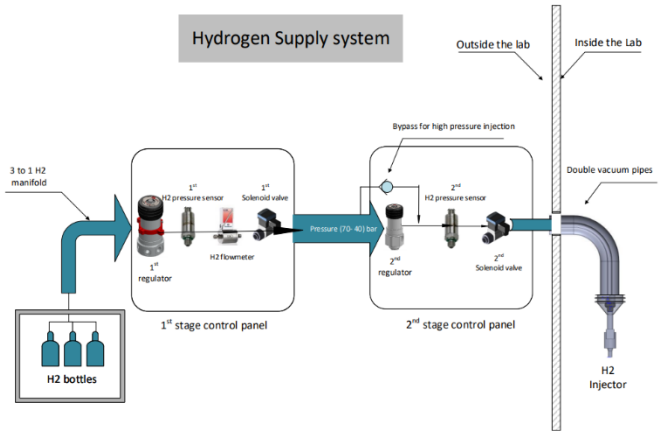

Figure 2. H_2 supply line

The properties of hydrogen that are of interest are presented in Table 2. Although the autoignition temperature of hydrogen is relatively high, the ignition energy of hydrogen-air mixtures is approximately one order of magnitude lower than that of hydrocarbon-air–air mixtures.

Table 2. Comparison of fuel proprieties between Hydrogen and Gasoline *[32]*.

Properties	**Units**	**Hydrogen**	**Gasoline**
Auto-ignition Temperature	K	858	550
Lower heating value	MJ/kg	119.93	44.2
Density	Kg/m^3	0.08	730
Molecular weight	g/mol	2.016	60-150
Flammability limits in air	vol%	4-75	1.4–7.6
Flame velocity	m/s	2.65-3.25	0.37–0.43
Specific gravity	-	0.091	0.71
Boiling point	K	20.2	230
Octane number	-	130	95
Mass diffusivity in air	cm^2/s	0.61	0.89
Adiabatic flame temperature (at stoichiometry)	K	2480	2580
Minimum ignition energy (at stoichiometry)	mJ	0.02	0.24
Stoichiometric air-to-fuel mass ratio	-	34.4	14.7
Flame velocity (at stoichiometry)	$m\ s^{-1}$	1.85	0.26

2.4 Emission Analysers

A HORIBA (MEXA-584L) was used to measure CO/CO2 and oxygen (O_2). A Cambustion DMS 500 fast particle analyser was employed to measure any PM emissions in terms of particle number and size. Also, Rotork Analysis Model 523 flame ionisation detection (FID) HC analysers were used to measure steady-state emissions. Furthermore, a fast NOx emissions analyser was connected to the back of the exhaust valves with a 1.2-meter emissions pipe to measure the instantaneous NO and NO_2 emissions [33]. Finally, the hydrogen concentration in the exhaust (H_2 slip) was measured by a V&F hydrogen analyser.

2.5 DAQ system

There are 138 input channels receiving signals from the sensors and measurement equipment in the engine test room. However, the sampling rate for each sensor depends on the sensor's priority and the reading's value. For instance, the in-cylinder, intake, and exhaust gas pressures are sampled in the crank domain, whilst the other sensor outputs are recorded in the regular time domain. Thus, a hybrid selection of NI cards encompasses fast and standard USB NI cards. These cards can automatically synchronise within the NI-based combustion analyser, Valieteck. Furthermore, it uses an NI to CANBus communication card to transfer signals from the ECU, as shown in Figure 3. The phenomenon of in-cylinder pegging is achieved by comparing the in-cylinder pressure value with the intake pressure from the fast response sensor at a crank domain degree of 100 before top dead centre firing (BTDCf). The TDC location is identified using an

encoder signal and calibrated during the motoring process and self-system check.

The indicated thermal efficiency is calculated from the Fuel's Lower heating value multiplied by the hydrogen flow rate. That is divided by the Indicated power, calculated from the in-cylinder pressure sensors and IMEP, as shown in equation 1.

$$ITE(\%) = \frac{Indecated\ Power\ (Kw).3600}{Fuelflow\left(\frac{Kg}{hr}\right).\text{CalorificValu}(\frac{\text{KJ}}{\text{Kg}})} \quad (1)$$

The assessment of combustion cyclic variability is determined by the coefficient of variation of indicated mean effective pressure (COV_{IMEP}) over 300 cycles, as per Equation 2.

$$COV_{IMEP}(\%) = \frac{\sqrt{\frac{\sum_{i=1}^{n}(IMEP_1 - IMEP_{mean})^2}{n-1}}}{IMEP_{mean}} \quad (2)$$

The lower net value (LNV) is introduced to identify partial combustion or misfiring instances, and it is calculated based on the ratio of the minimum IMEP to the averaged IMEP over 300 cycles, as shown in Equation 3.

$$LNV_{min}(\%) = \frac{IMEP_{min}}{IMEP_{av}} * 100 \quad (3)$$

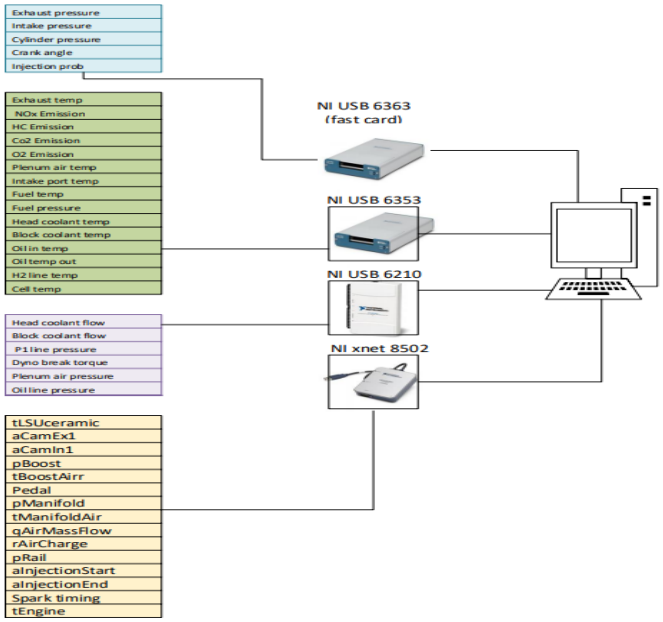

Figure 3. Schematic of DAQ system

3. Test Methodology

The experimental testing consisted of running an engine using two independent hydrogen injection systems, namely port fuel injection and central direct injection, at three different engine speeds (1500, 2000 and 3000 rpm), different engine loads, and relative air-to-fuel ratios (λ).

Table 3 summarises the engine test conditions for the three investigated experiments, namely λ sweep test, engine load sweep test and cam envelope sweep test. The first experiment (λ sweep) consisted of investigating the effect of λ values (from 1.5 to above 3) and was conducted at a fixed engine load of 1000 kPa IMEP (simulates mid-load) and fixed intake and exhaust cam positions of 97 CAD ATDCg and 102 CAD BTDCg, respectively. The second experiment (engine load sweep) was conducted for a range of engine loads from 400 kPa to 1600 kPa (low to high engine operation) at a fixed λ of 2.75 and fixed intake and exhaust cam positions of 97 CAD ATDCg and 102 CAD BTDCg, respectively. The last experiment (cam envelope sweep) was performed for a wide range of both intake (75-120 CAD ATDCg) and exhaust (80-125 CAD BTDCg) cam timings at a fixed λ of 2.75, fixed engine load and speed of 1000 kPa IMEP and 2000 rpm, respectively.

For accurate control, the intake temperature was fixed at 38 degrees Celsius using an inline air heater with PID control within 0.3 degrees. The oil and water coolant temperatures were fixed at 90 degrees with external heaters, and PID correlates with a 3-degree variation.

The injection pressure and start of injection were typically set at 3000 kPa and 150 CAD BTDCf, respectively. The injection pressure was reduced to 1000 kPa for engine loads below 800 kPa IMEP to achieve stable combustion. The PFI was held constant at 1000 kPa, and the end of injection was fixed at 200 CAD BTDCf to ensure that the PFI took place after the intake valves opened to minimise the hydrogen buildup in the intake that could cause backfire.

The limits of the highest average in-cylinder pressure and maximum pressure rise rate (R_{max}) were set to 12000 kPa and 600 kPa/CAD. COV_{IMEP} of 1.5% was used to determine stable engine operation. The combustion phasing (50%MB) was set between 8 and 10 CAD ATDCg for optimal combustion.

The λ values were measured by two wide-band relative air-fuel ratio sensors in the exhaust line, calibrated with O_2 measurements from the Horiba emission analyser, and then compared to a λ calculated from hydrogen flow rate minus the H2 slip and air flow rate. Finally, all three testing sets have been conducted using full DI and then repeated with the exact operating conditions using PFI.

Table 3. Engine test conditions

Engine parameters	**Unit**	**λ sweep test**	**Engine load sweep test**	**Cam envelope sweep test**
Engine Speed	rpm	1500, 2000, 3000	1500, 2000, 3000	2000
Engine Load	kPa	1000	SWEEP	1000
λ	-	SWEEP	2.75	2.75
Intake Cam positions	ATDCg	97	97	SWEEP
Exhaust Cam positions	BTDCg	102	102	SWEEP

Start of injection DI	BTDCf	150	150	150
End of injection PFI	BTDCf	200	200	200
Injection pressure DI	kPa	3000	1000 at low load, 3000 from 800 kPa IMEP	3000
Injection pressure PFI	kPa	1000	1000	1000

4. Results and Discussions

This study examines an SI engine's performance and emissions characteristics fueled by DI or PFI. The λ values were adjusted at different speeds to determine the optimal λ for each technique. Once the optimal λ was identified, it was set at various engine speeds during load variations.

4.1 Effect of Lambda on PFI and DI H2 engine performance and emissions at a constant mid- load.

The first experiment was carried out to evaluate the performance and emissions characteristics of the H2 engine operating at a fixed load of 1000 kPa IMEP and three engine speeds of 1500rpm, 2000rpm and 3000rpm. The relative air-to-fuel ratio λ was varied to determine the minimum λ and the lean-burn limit for PFI and DI operations.

As shown in the top graph of Figure 4, in most cases, the 50%MB was between 8-10 CAD after the TDC for the maximum efficiency when the spark ignition timing was set to MBT (minimum ignition advance for Best Torque), except with the richest and leanest mixtures. When the λ value was reduced to be less than 1.5 at 2000rpm, the combustion became significantly faster and hence the spark timing had to be retarded, as shown in Figure 6, in order to keep the R_{max} below the limit of 600 kPa per crank angle shown in Figure 5. The results in Figure 4 show that the maximum thermal efficiency was achieved within the λ range of 2.5 to 3.5. It is noted that the DI operation had slightly higher ITE than PFI operation.

For both PFI and DI, the lean-burn limit was identified by the LNV_{min} given by Eq.3 . As shown in Figure 5, the drop in LNV_{min} and sudden rise in COV_{IMEP} at 3000 rpm DI λ 3.75 was caused by one partial burn cycle amongst 300 cycles. Overall, PFI and DI operations were characterised by stable combustion with less than 1.5% variate the injection over a wide range of λ values. The cyclic variation was slightly increased when the λ was increased toward the lean operation limits. However, at the rich operation points (low λ), the PFI operation experienced a backfire in the intake, thanks to the ignition of hydrogen in the intake by the hot burnt gas escaping the cylinder during the valve overlap period. As a result, PFI operation was restricted to a minimum λ of 1.5.

In comparison, the DI operation could be operated with lower λ without backfire because of the absence of hydrogen in the intake system when hydrogen was injected directly into the cylinder later in the intake process at a much higher injection pressure of up to 4,000 kPa. The bottom graph in Figure 5 shows that the pressure rise rate increased with lower λ due to faster combustion. In order to keep R_{max} below the limit of 600 kPa per crank angle, the spark timing was retarded.

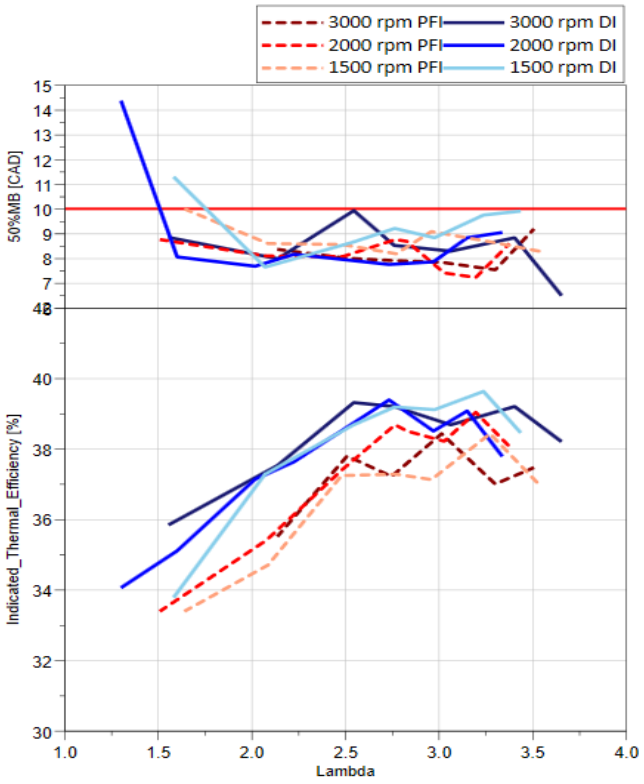

Figure 4. The thermal efficiency of direct injection (DI) and port fuel injection (PFI) systems at different λ values and the 50% mass burn rate

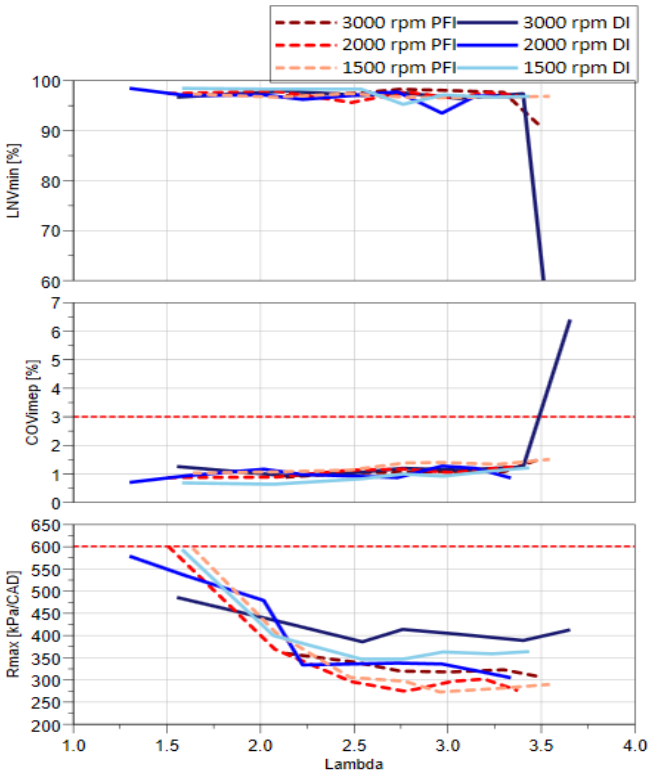

Figure 5. operational constraints associated with different speeds and λ values in DI and PFI systems

Figure 6 shows the spark timings and the burn durations. All the spark timings were at MBT other than the operation with λ lower than 1.5 where the sparking was retarded after top dead centre firing (ATDCf) to maintain the pressure rise rate within 600 kPa per crank angle limit. In the case of PFI operation, the MBT timings became more advanced with the engine speed as expected when both the initial flame development (0-10%) and the main combustion duration (10-90%) increased in terms of crank angles as expected. The DI operation followed the same trend when λ was less than 2, above which 2000rpm operation exhibited longer combustion duration and more advanced spark timings than the other engine speed. Direct injection operation generally were characterised by longer combustion durations than the equivalent PFI operation.

PFI and DI hydrogen engine operations produced zero CO2, CO, and HC emissions throughout all experiments. Figure 7 shows NOx emissions was less than 10 ppm from λ=3.0 to 3.5 and no more than 50 ppm between λ= 2.75 to 3. It increased rapidly from λ 2.5 to 1.5. At 1500rpm, the DI operation produced higher NOx emissions below λ 2.0, probably due to burning a slightly richer mixture that was more likely to be formed during the direct injection operation. However, PFI operation resulted in more H_2 concentration in the engine's exhaust gas than the DI operation, which is thought to be due to more hydrogen being trapped in the crevices during the compression stroke. Additionally, more H_2 was measured at the lower engine speed during the PFI operation, which was hardly affected by the engine speed when hydrogen was injected directly into the cylinder.

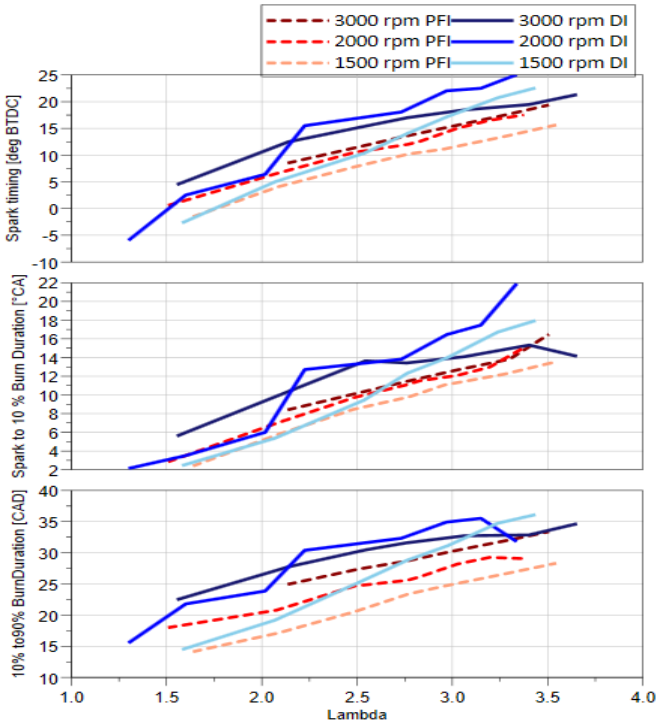

Figure 6. The parameters of spark ignition and burn duration

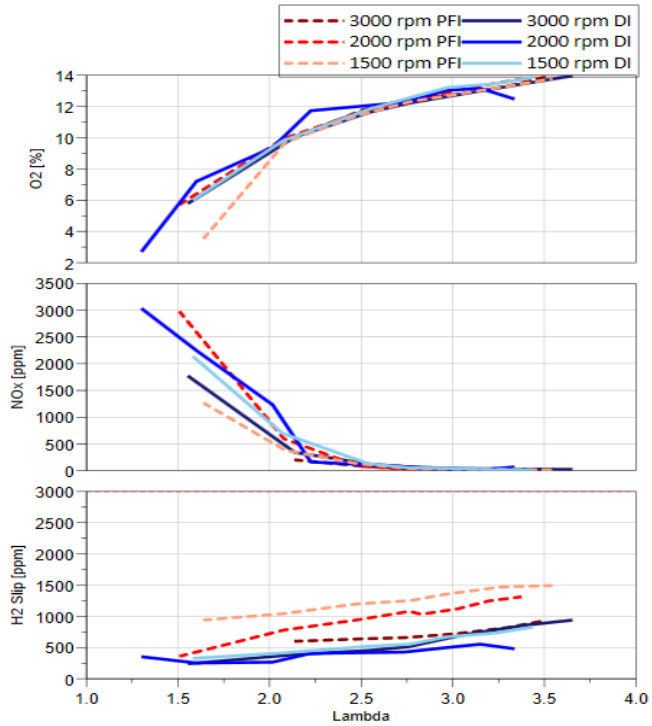

Figure 7. The main three outputs from the exhaust line, Oxygen, NOx, and H_2 slip

In order to quantify the error of measured λ by the lambda sensors in the exhaust due to the presence of unburned fuel, measurements of exhaust gas components can be used to calculate the actual air-to-fuel ratio and λ in the cylinder in a controlled experimental setting. To assess the influence of H_2 slip on the measured emissions-based λ, a particular air-fuel ratio equation for H_2 was formulated based on Equation 4 [34].

$$H_2 + A\left[O_2 + {}^{79}/_{21}\,N_2 + Z.(H_2O)\right] \rightarrow c.H_2O + d.H_2 + e.O_2 + f.NO + g.N_2 \quad (4)$$

By utilising the atom balances for hydrogen and oxygen, along with the equations for emissions volume concentration, a solution for variable A can be obtained.

$$A = \frac{1 - [H_2] + [O_2] + {}^{1}/_{2}\,[NO]}{z - [O_2]\left(\frac{200}{21} + 2.z\right) - [NO]\left(\frac{200}{42} + z\right) + [H_2]\left(\frac{79}{21} + z\right)} \quad (5)$$

$$z = \frac{100}{21}.HR.\frac{M_{Air}}{M_{H_2O}} \quad (6)$$

$$AFR = 2.A.AFR_{stoich} \quad (7)$$

The wet exhaust volume concentrations for O_2, H_2, and NOx are denoted as $[O_2]$, $[H_2]$, and $[NO]$, respectively. HR represents the humidity ratio, whereas M_{air} and M_{H2O} are the molar masses for air and water, respectively.

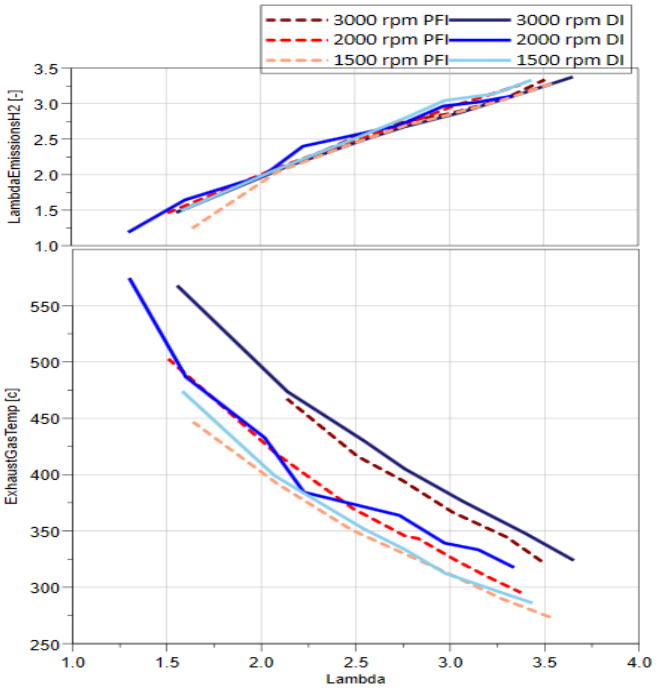

Figure 8. The relationship between the estimated and measured λ emission based on λ values and the exhaust gas temperature

The upper graph in Figure 8 shows the relationship between the in-cylinder λ values based on measured emissions and the λ values by the lambda sensors. Both λ values were consistent until λ 3, except at the lowest λ at 1500rpm due to a dip in O_2 concentration by the lambda sensor. Near the lean-burn limits beyond λ 3, the in-cylinder λ values were slightly lower than the lambda sensor readings due to the decreased accuracy of the lambda sensor with higher O_2 concentrations. As shown in the lower graph in Figure 8, the DI operation was characterised by slightly higher exhaust gas temperatures due to the slower combustion and delayed end of combustion.

The results of the λ sweep test conducted at various speeds indicate that the DI hydrogen operation exhibited a slightly higher ITE than the PFI operation due to the lower pumping loss and less hydrogen slip emissions. PFI and DI hydrogen engine operations produced no CO_2, CO, or HC emissions. Both injection strategies enabled stabled engine operation to be achieved across a wide range of λ values, though the occurrence of backfire limited the PFI operation to λ 1.5 or above.

Based on the findings observed in the λ sweep test, it was determined that the ideal operational λ range for achieving minimal NOx emissions, optimal thermal efficiency, and reduced H_2 slip lies between λ 2.75 and 3. Therefore, λ 2.75 was selected for the additional engine testing conducted in different engine operating conditions, as it required less air boosting for high load and maintained the Nox emissions in the low region.

4.2 Comparison of PFI and DI hydrogen engine performance and emission with load sweep operating conditions at a fixed lambda

This experiment assessed PFI and DI strategies' performance and emissions characteristics at different engine speeds and loads at a fixed λ 2.75. Figure 9 depicts ITE for PFI and DI strategies at different engine loads and speeds. Figure 10 illustrates the operating constraints, namely 50%MB, LNV_{min}, COV_{IMEP} and R_{max}, while Figures 12 and 13 show the emissions and the intake air pressure, respectively. Finally, Figure 14 compares measured and calculated λ and O_2 concentrations.

Figure 9 indicates that ITE increased with engine load for both PFI and DI operation, with an efficiency peak occurring from 1000 kPa onwards due to the reduced pumping work. DI operation demonstrated higher ITE than PFI, ranging from approximately 2.5 percentage points at lower loads to 1.5 percentage points at higher loads. This is thought to be a result of increased volumetric efficiency generated by higher injection pressures offered by the DI technology, as reported by other authors [28, 29]. Furthermore, engine speed affected ITE in both systems, especially at low and medium engine loads, with lower speeds resulting in higher thermal efficiencies up to the load point of 1000 kPa, which corresponded to the wide-open-throttle position.

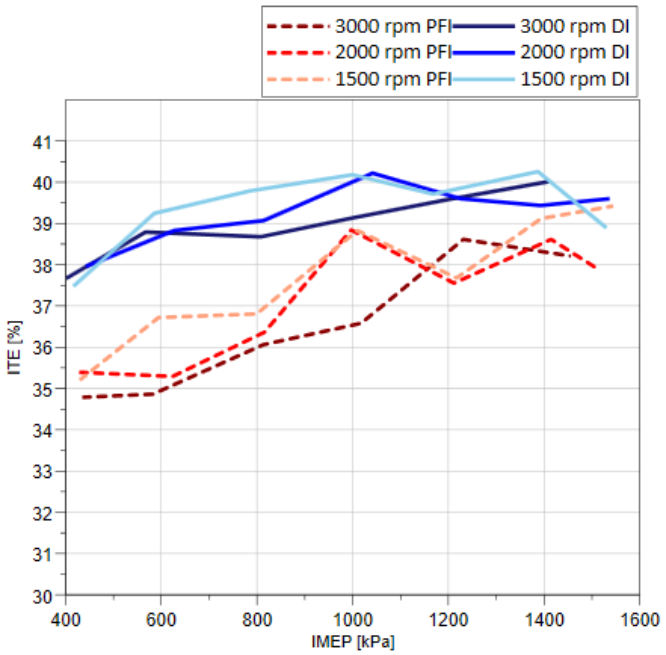

Figure 9. Indicated thermal efficiency of DI and PFI systems at different engine loads and speeds

As shown in Figure 10, both PFI and DI engines were characterised by very stable combustion from low to high load operations with COV_{IMEP} remaining below 1.5% and 50 50%MB between 8-10 CAD after TDC, except for the direct injection at very high engine load (IMEP > 1400 kPa). This exception was caused by the retarded 50%MB to keep R_{max} below 500 kPA/CAD using retarded spark timing from MBT, as shown in Figure 11. An anomaly of the LNV_{min} minimum peak was seen in Figure 10 at 800 kPa IMEP with the DI system, but no effect on COV_{IMEP} was present. The LNVmin minimum peak was found to be caused by one partial burn cycle. During the experiments, the DI injection pressure had to be adjusted (lowered to 1000 kPa) for engine loads under 600 kPa, as higher injection pressures appeared to cause increased cycle-to-cycle variations. This could be caused by several factors, such as the cyclic variation in fuel injection and mixture formation due to changes in in-cylinder flows.

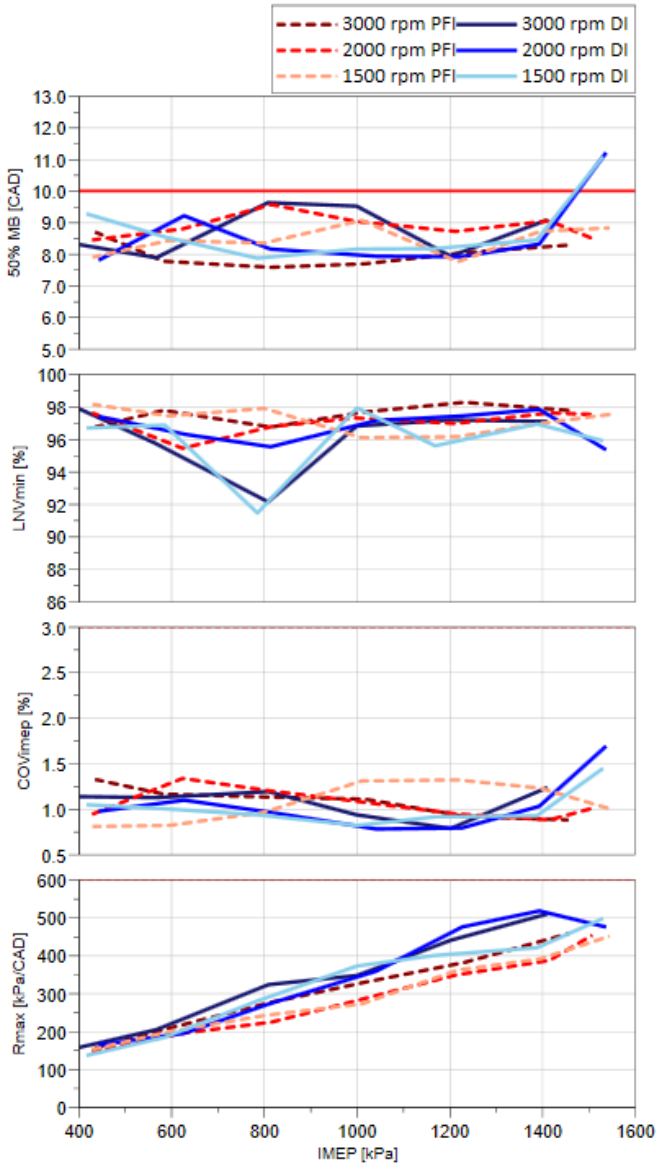

Figure 10. Operational constraints associated with DI and PFI systems at different engine loads and speeds

Similar to the λ sweep experiment results in the previous section, central DI operation were characterised by longer burn durations than PFI for both the spark to 10% and 10% to 90% of the mass fraction burned period. Additionally, the combustion duration increased, and the MBT spark timings became more advanced as the engine load was increased. Such trends are opposite to the SI gasoline engine, which has a shorter combustion duration at a higher load as the flame speed is faster when the gas temperature and pressure are higher, resulting in less spark advance. These results may indicate that the in-cylinder pressure and temperature have much less effect on the hydrogen flame speed than the gasoline combustion and that the hydrogen combustion is slowed down at higher gas pressure. Another reason could be the stratification of the in-cylinder charge resulted from more retarded spark timing; however, further optical measurements should be considered.

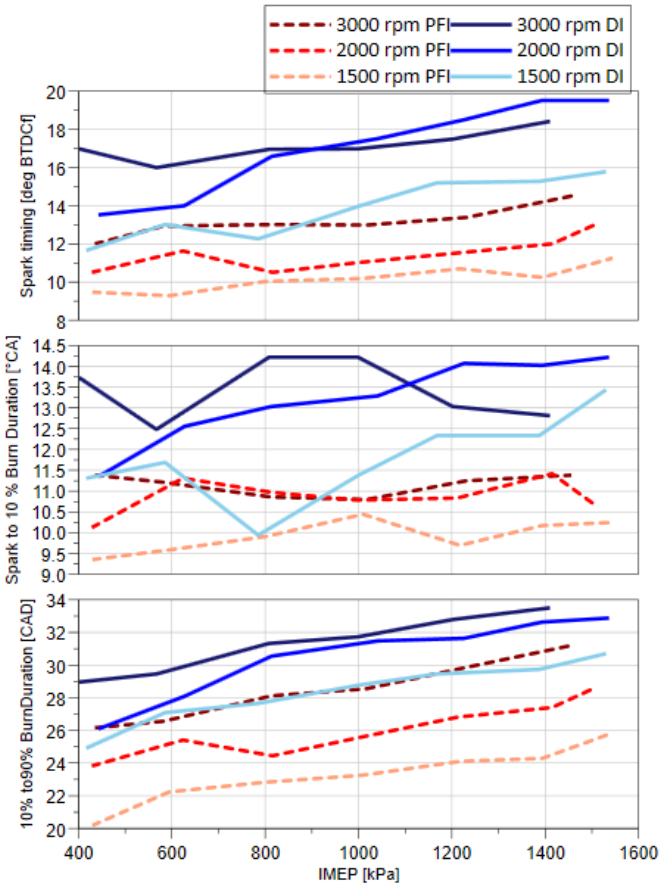

Figure 11. The parameters of spark ignition and burn duration of DI and PFI systems at different engine loads and speeds

Figure 12 shows that NOx emissions started to rise when the load was above 1200 kPa IMEP for the DI operation, although remaining significantly low (below 150 ppm). This occurrence was likely caused by the partially stratified charge in the cylinder when the end of injection was delayed to enable more hydrogen to be injected. The combustion of a slightly richer mixture would lead to more NO formation and emissions. Similar to the results in the previous section, the exhaust gas temperatures of the DI operation were higher thanks to the delayed combustion and the higher H2 slip from the PFI operation was probably caused by higher H2 trapped in the crevice volume.

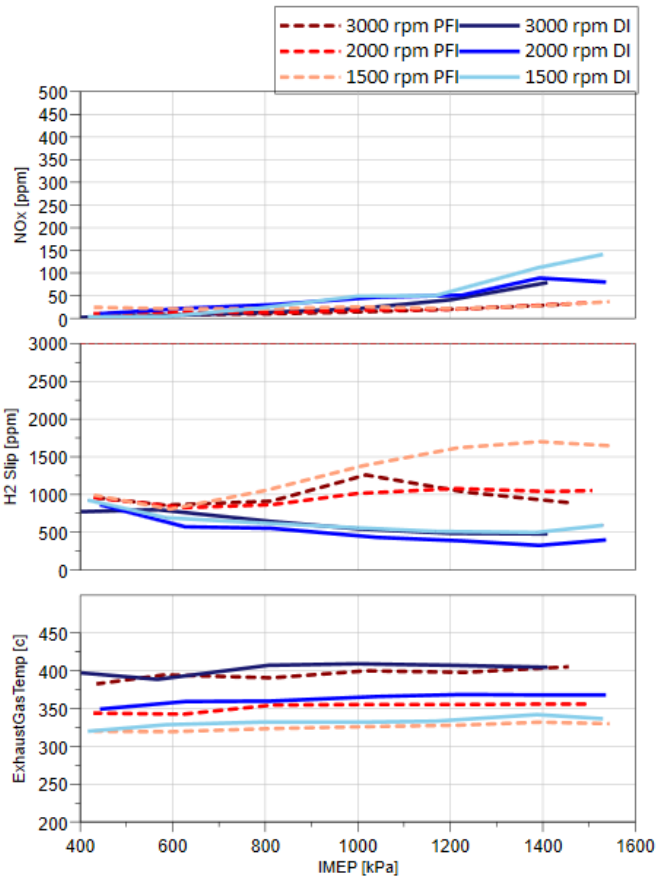

Figure 12. Exhaust emissions and temperatures generated by DI and PFI systems at different engine loads and speeds

The intake air pressure was another significant difference found during the experiment between DI and PFI systems. As illustrated in Figure 13, PFI requires more boosting pressure to achieve the same operating conditions (λ and engine load) as DI. This can be explained by the fact that PFI supplied hydrogen in the manifold during the intake stroke and displaced the airflow at the intake pressure. By contrast, the direct injection of hydrogen occurred within the cylinder at the beginning of the compression stroke (150 CAD before TDC) without displacing the pre-existing air in the cylinder after the intake valves had been closed. Consequently, a higher boosting pressure was required for the PFI operation in order to maintain an equivalent air and fuel mixture within the cylinder, compared to the DI operation.

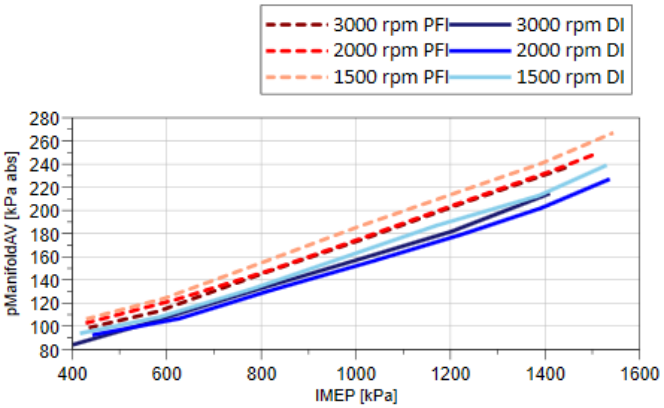

Figure 13. Intake air pressure of DI and PFI systems at different engine loads and speeds

The previous section demonstrated that both measured and calculated relative air-fuel ratios were aligned for different λ values, except for very lean operation. Therefore, it was essential to compare the measured λ by S1/S2 with the calculated λ and O_2 concentration measured by the Horiba analyser since λ was one of the constants of this experiment, as described in the Methodology section. As shown in Figure 13, both λ values and O_2 had the same values when the engine load was changed, confirming the accuracy of this experiment's results.

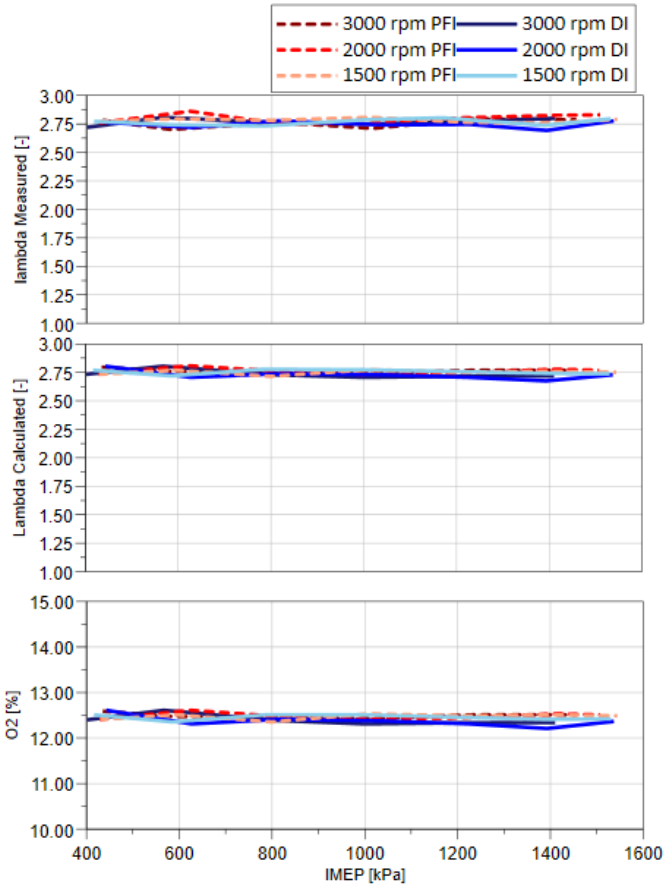

Figure 14. Measured and calculated λ as well as O_2 concentration generated by DI and PFI systems at different engine loads and speeds

The engine load sweep test results at various speeds show a slight difference between the performance of DI and PFI systems. In addition, the DI strategy has a slightly higher ITE than the PFI strategy. Similar to λ values sweep experiments, both injection strategies exhibit excellent combustion stability across the wide engine loads and speeds tested. Nevertheless, an essential distinction between the two injection systems is the boosting pressure, with DI requesting lower intake pressure and hence less demand on the boosting system.

4.2 Investigation of the benefit of the high-pressure late injection of the DI vs PFI over a full cam envelope.

The results from the previous two sections have demonstrated the beneficial effects of DI over PFI hydrogen in terms of performance and emissions. This section investigates the synergy between DI and variable valve timing controls. In this test, the speed and load were fixed at 2000 rpm and 1000 kPa IMEP. The λ was kept constant at 2.75 to eliminate the influence of the relative air-fuel ratio on the performance and emissions. The timing of the intake valve maximum lift was shifted from 117 degrees after top dead centre gas exchange (ATDCg) to 87 degrees ATDCg with 10 degrees step, and the exhaust cams shifted from 122 to 92 degrees before top dead centre gas exchange (BTDCg), as shown in Figure 15. The experiments comprised 16 matrix points from minimum to maximum overlap.

The larger intake and exhaust valve overlap near the TDC intake, enabling an enhanced scavenging effect at high-load operation. By completing this matrix for both PFI and DI operations and studying the highest possible valve overlap setup, we can assess the effect of alternative valve timings on hydrogen performance and emission parameters with both injection methods. Additionally, the results would be used to determine the optimal cam configuration for each injection system and assess the potential benefits of the DI in terms of cam overlap compared to PFI.

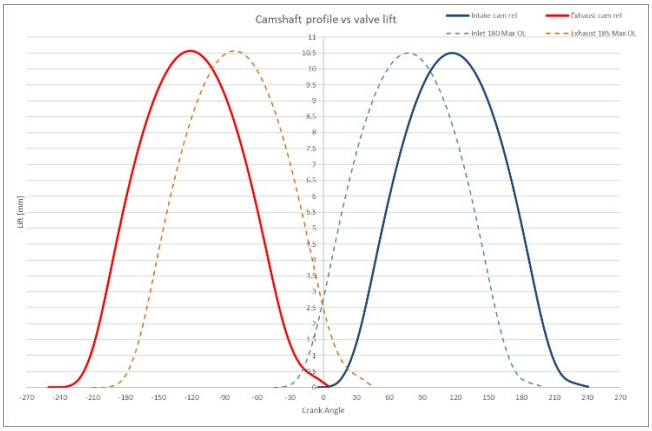

Figure 15. Intake and exhaust cam profile with maximum and minimum overlap

Figure 16 illustrates the relationship between H_2 slip in the exhaust line and the intake and exhaust cam envelope. For PFI, H_2 slip increased with more valve overlap in the bottom left region and went up to more than 3000 ppm with the retarded exhaust cam peak at 92 CAD BTDCg and the advanced intake cam at 82 CAD ATDCg. However, to protect the λ sensors from overheating by burning unburned hydrogen (H2 slip) in the exhaust gas, the exhaust and intake cams during the PFI operation were limited to 102 CAD BTDCg and 97 CAD ATDCg, respectively. This configuration had an H_2 slip value of 1000 ppm, similar to the prior λ sweep test value. The start of direct hydrogen injection was set at 210 CAD ATDCg after the complete closure of the intake valve, allowing for optimal overlap. When comparing the PFI and DI systems, it can be observed that the DI system generated about 50% less H_2 slip across the tested valve timing matrix. It is worth noting that a minor non-linear variation in H2 slip in the Di, which is caused by a reduction in exhaust timing of less than 200 PPM, may be attributed to the boundary conditions of the chamber and the state of the mixture.

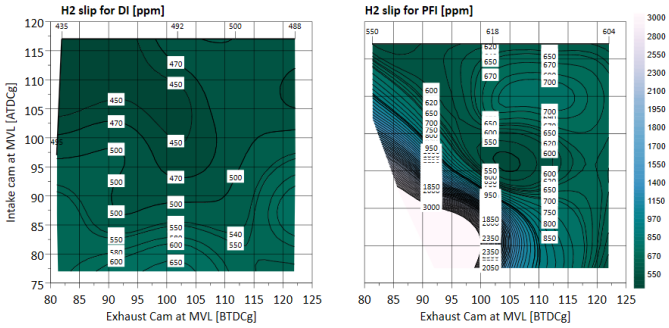

Figure 16. H_2 slip of each injection system over the valve timing matrix

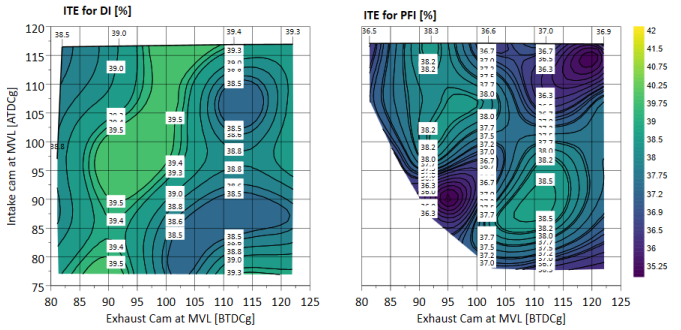

Figure 17. Indicated thermal efficiency of each injection system over the valve timing matrix

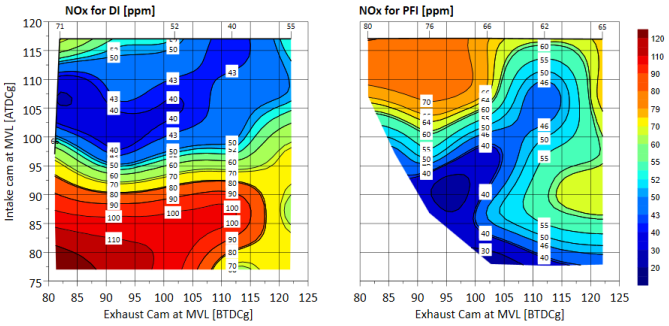

Figure 18. NOx emissions of each injection system over the valve timing matrix

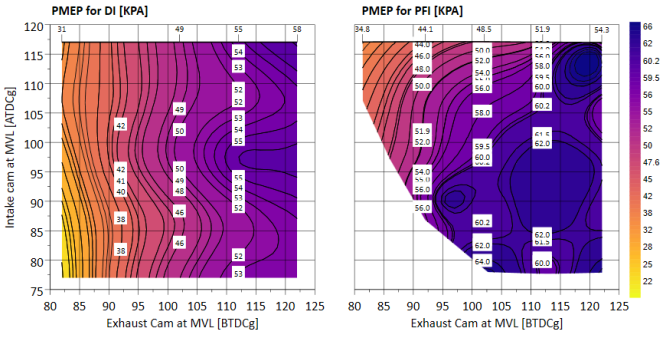

Figure 19. PMEP of each injection system over the valve timing matrix

Figure 17 compares the thermal efficiencies of each injection system across the cam matrix. The cam timings had more impact on the performance of the PFI operation with a fixed end of injection at 200 CAD BTDCf. The ITE of the PFI operation experienced a decline of 4% at the peak overlap period, primarily attributed to the short-circuiting of hydrogen through the exhaust valves. The maximum thermal efficiency for the PFI system was achieved when the maximum lift of exhaust valves was at 102 CAD BTDC and the maximum lift of intake valves was at an angle of 82 CAD ATDC. Therefore, these valve times were adopted when the other tests were performed to compare the DI and PFI operations.

Figure 18 indicates the impact of the valve timings and their overlap on NOx emissions. The PFI exhibited lower NOx emissions, consistent with the previously presented results. The peak level of NOx during the PFI operation was observed when the ITE was highest, thanks to higher combustion temperature. The NO emissions significantly decreased towards the maximum overlap period region in the bottom left, where more H2 slip was found. In contrast, the DI system exhibits slightly higher NOx emissions, though all below 100pm, probably caused by the higher temperature combustion in the partially stratified mixture. The NO emissions appeared to increase with the earlier closure of the intake valves, thanks to the slightly increased effective compression ratio and higher gas temperature. The maximum NO emissions were with the maximum overlap setting.

Figure 19 highlights the noticeable difference in PMEP (Pumping Mean Effective Pressure) between the PFI and DI hydrogen engines. The higher PMEP values of the PFI operation were caused by the increased compression work due to higher intake pressure, as shown in Figure 13, and hence increased compression work. It also helps to explain the lower ITE values of PFI than those of DI operation. Furthermore, the increasing PMEP values with the earlier exhaust valve opening seem consistent with the decreasing ITE values from the left to the right in the graphs.

5 Conclusions

The present study has carried out an evaluation of the performance and emissions characteristics of both H2 DI and PFI systems. The assessment included investigations into the influence of different lambda values and loads at various engne speeds to examine each system's performance enhancements and operational capabilities. Additionally, the study explored the potential advantages of incorporating delayed and high-pressure injection into direct injection systems, particularly in combination with the optimised valve overlap setups.

The main findings can be summarised as follows:

(1) The current downsized SI gasoline engines can be readily converted to operate with hydrogen using either a DI and a PFI fuelling system. Compared to gasoli engines, both PFI and DI hydrogen engines exhibit consistently higher thermal efficiencies due to their lean burn operation within the lambda range of 2.5 to 3.7. While the PFI H2 engine can operate within a lambda range of approximately 1.5 to 3.7, the DI H2 engine can function within a much broader lambda range, including stoichiometric mixture, without encountering any backfire issues.

(2) The DI H2 operation exhibited superior performance compared to PFI across the entire load and lambda sweep in terms of thermal efficiency. This can be attributed to the lower pumping works and reduced H2 slip in the exhaust.

(3) Additionally, H2 DI opeation required less boosting than the PFI setups, thanks to its higher volumetric efficiency. This translates to reduced pumping work and lower demand on the boosting system.

(4) Both DI and PFI operation produced zero emissions of carbon dioxide (CO2), hydrocarbons (HC), and carbon monoxide (CO). Additionally, both systems demonstrate ultra-low and near-zero NOx emissions from lambda 2.5 to 3.7.

(5) The DI H2 system could be used with positive valve overlap for improved scavenging effects with little hydrogen slip. Further, a higher injection pressure of 40 bar contributes to an enhanced combustion process in high-load conditions.

(6) The parameter of engine stability, LNV_{min} was found to display a higher sensitivity and better representation of the overall engine ability compared to COV_{IMEP}. Both the DI and PFI operations were found to exhibit exemplary stability across a wide range of lambda up to lean limits, where a sudden partial burn occurred without any initial sign of instability.

Additional studies on the potential benefits of passive and active pre-chamber have also been conducted, and the results will be presented in a future paper.

References

[1] Administration of Joseph R Biden, "Executive Order 14037- Strengthening American Leadership in Clean Cars and Trucks," Office of the Federal Register, National Archives and Records Administration, 2021.

[2] European Parliament and the Council, "Regulation (EU) 2023/851 of the European Parliament and of the Council amending Regulation (EU) 2019/631 as regards strengthening the CO2 emission performance standards for new passanger cars and new light commercial vehicles," Official Journal of the European Union, 2023.

[3] K. Wrobel, J. Wrobel, W. Tokarz, J. Lach, K. Podsadni and A. Czerwinski, "Hydrogen Internal Combustion Engine Vehicles: A Review," *Energies,* vol. 15, no. 23, 2022.

[4] R. Kothari, D. Buddhi and R. L. Sawhney, "Comparison of environmental and economic aspects of various hydrogen production methods," *Renewable and Sustainable Energy Reviews,* vol. 12, no. 2, pp. 553-563, 2008.

[5] G. Conway, "Life-Cycle Analysis for the Automotive Sector," in *Engines and Fuels for Future Transport*, G. Kalghatgi, A. K. Agarwal, F. Leach and K. Senecal, Eds., Singapore, Springer, 2022, pp. 103-131.

[6] S. Verhelst, "Recent progress in the use of hydrogen as a fuel for internal combustion engines," *International Journal of Hydrogen Energy,* vol. 39, no. 2, pp. 1071-1085, 2014.

[7] J. Hall, A. Harrington, A. Cooper, M. Bassett, N. Hiett, D. Richardson, A. Martens and S. Sapsford, "Technical Assessment of the Feasibility of the use of Bio-Gasoline as a Drop-In Gasoline Fossil Fuel Replacement," SAE Technical Paper 2022-01-1087, 2022.

[8] M. Mohamed, H. Zhao, A. Harrington and J. Hall, "Experimental Investigation of Combustion Characteristics, Performance, and Emissions of a Spark Ignition Engine with 2 nd Generation Bio-Gasoline and Ethanol Fuels," SAE Technical Paper 2023-01-0339, 2023.

[9] A. Harrington, J. Hall, M. Bassett, E. Lu and H. Zhao, "Combustion Characteristics and Exhaust Emissions of a Direct Injection SI Engine with Pure Ethanol and Methanol in Comparison to Gasoline," SAE Technical Paper 2022-01-1089, 2022.

[10] A. Harrington, J. Hall, M. Bassett and A. Cooper, "Effect of Jet Ignition on Lean Methanol Combustion Using High Compression Ratio," SAE Technical Paper 2023-01-0319, 2023.

[11] P. K. Bose and D. Maju, "An experimental investigation on engine performance and emissions of a single cylinder diesel engine using hydrogen as inducted fuel and diesel as injected fuel with exhaust gas recirculation," *International Journal of Hydrogen Energy,* vol. 34, no. 11, pp. 4847-4854, 2009.

[12] S. Sharma and S. K. Ghoshal, "Hydrogen the future transportation fuel: From production to applications," *Renewable and Sustainable Energy Reviews,* vol. 43, pp. 1151-1158, 2015.

[13] S. Jilakara, J. Vaithianathan, V. Ramakrishnan, S. Natarajan, G. P. Subash, M. Abraham, J. Krishnan and L. M. Das, "An Experimental Study of Turbocharged Hydrogen Fuelled Internal Combustion Engine," *SAE Int. J. Engines,* vol. 8, no. 1, pp. 314-325, 2015.

[14] L. Wang, H. Li, Z. Huang, L. Wang and W. Chen, "Impact of hydrogen direct injection on engine combustion and emissions in a GDI engine," *Advances in Mechanical Engineering,* vol. 15, no. 9, 2023.

[15] Z. Stępień, "A Comprehensive Overview of Hydrogen-Fueled Internal Combustion Engines: Achievements and Future Challenges," *Energies,* vol. 14, no. 20, 2021.

[16] L. Jingding, G. Linsong and D. Tianshen, "Formation and restraint of toxic emissions in hydrogen-gasoline mixture fueled engines," *International Journal of Hydrogen Energy,* vol. 23, no. 10, pp. 971-975, 1998.

[17] H. Fayaz, R. Saidur, N. Razali, F. S. Anuar, A. R. Saleman and M. R. Islam, "An overview of hydrogen as a vehicle fuel," *Renewable and Sustainable Energy Reviews,* vol. 16, no. 8, pp. 5511-5528, 2012.

[18] S. Verhelst and T. Wallner, "Hydrogen-fueled internal combustion engines," *Progress in Energy and Combustion Science,* vol. 35, no. 6, pp. 490-527, 2009.

[19] X. Tang, D. M. Kabat, R. J. Natkin, W. Stockhausen and J. Heffel, "Ford P2000 hydrogen engine dynamometer development," SAE paper 2002-01-0242, 2002.

[20] T. Wallner, "Efficiency and Emissions Potential of Hydrogen Internal Combustion Engine Vehicles," SAE Technical Paper, 2011.

[21] C. M. White, R. R. Steeper and A. E. Lutz, "The hydrogen-fueled internal combustion engine: a technical review," *International Journal of Hydrogen Energy,* vol. 31, no. 10, pp. 1292-1305, 2006.

[22] L. M. Das, "Hydrogen-oxygen reaction mechanism and its implication to hydrogen engine combustion," *International Journal of Hydrogen Energy,* vol. 21, no. 8, pp. 703-715, 1996.

[23] Q.-h. Luo, J.-B. Hu, B.-g. Sun, F.-s. Liu, X. Wang, C. Li and L.-z. Bao, "Experimental investigation of combustion characteristics and NOx emission of a turbocharged hydrogen internal combustion engine," *International Journal of Hydrogen Energy,* vol. 44, no. 11, 2019.

[24] S. J. Navale, R. R. Kulkarni and S. S. Thipse, "An experimental study on performance, emission and combustion parameters of hydrogen fueled spark ignition engine with the timed manifold injection system," *International Journal of Hydrogen Energy,* vol. 42, no. 12, pp. 8299-8309, 2017.

[25] B. Nagalingam, M. Dubel and K. Schmillen, "Performance of the supercharged spark ignition hydrogen engine," SAE Paper 831688. 1983., 1983.

[26] M. Berckmüller, H. Rottengruber, N. Eder, N. Brehm, G. Elsässer, G. Müller-Alander and C. Schwarz, "Potentials of a Charged SI-Hydrogen Engine," SAE Technical Paper 2003-01-3210, 2003.

[27] Z. Yang, F. Zhang, L. Wang, K. Wang and D. Zhang, "Effects of injection mode on the mixture formation and combustion performance of the hydrogen internal combustion engine," *Energy,* vol. 147, no. 15, pp. 715-728, 2018.

[28] Z. Sun, J. Hong, T. Zhang, B. Sun, B. Yang, L. Lu, L. Li and K. Wu, "Hydrogen engine operation strategies: Recent progress, industrialisation challenges, and perspectives," *International Journal of Hydrogen Energy,* vol. 48, no. 1, pp. 366-392, 2023.

[29] S. Verhelst, J. De Landtsheere, F. De Smet, C. Billiouw, A. Trenson and R. Sierens, "Effects of Supercharging, EGR and Variable Valve Timing on Power and Emissions of Hydrogen Internal Combustion Engines," *SAE Int. J. Engines,* vol. 1, no. 1, pp. 647-656, 2009.

[30] C. Park, Y. Kim, S. Oh, J. Oh and Y. Choi, "Effect of the operation strategy and spark plug conditions on the torque output of a hydrogen port fuel injection engine," *International Journal of Hydrogen Energy,* vol. 46, no. 74, pp. 37063-37070, 2021.

[31] A. Mohammadi, M. Shioji, Y. Nakai, W. Ishikura and E. Tabo, "Performance and combustion characteristics of a direct injection SI hydrogen engine," *International Journal of Hydrogen Energy,* vol. 32, no. 2, pp. 296-304, 2007.

[32] C. M. White, R. R. Steeper and A. E. Lutz, "The hydrogen-fueled internal combustion engine: a technical review," *International Journal of Hydrogen Energy,* vol. 31, pp. 1292-1305, 2006.

[33] "Fast Response Portable NO and NO2 Analyzer | CLD50," Cambustion, 2022. [Online]. Available: https://www.cambustion.com/products/engine-exhaust-emissions/nox-analyzers/cld50-ambient-and-engine-nox. [Accessed 20 10 2023].

[34] N. Peters and M. Bunce, "Lambda Determination Challenges for Ultra-Lean Hydrogen-Fueled Engines and the Impact on Engine Calibration," SAE Technical Paper 2023-01-0286, 2023.

Contact Information

Mr Mohamed Mohamed
Doctoral researcher
Centre for Advanced Powertrain and Fuels
College of Engineering, Design and Physical Sciences
Brunel University London Uxbridge UIB8 3PH
email: moahmed.mohamed@brunel.ac.uk

Mr Kevin Longo
Doctoral researcher
Centre for Advanced Powertrain and Fuels
College of Engineering, Design and Physical Sciences
Brunel University London Uxbridge UIB8 3PH
email: kevin.longo@brunel.ac.uk

Professor Hua Zhao
Centre for Advanced Powertrain and Fuels
College of Engineering, Design and Physical Sciences
Brunel University London Uxbridge UIB8 3PH
email: hua.zhao@brunel.ac.uk

Acknowledgements

UKRI has funded this research, and the MAHLE Powertrain provides the experimental power unit. Clean Air Power and Phinia provide the Hydrogen Di and PFi injectors, and Cambustion provides the fast

NOx emission analyser. Ford Motor Company has managed this project.

ZEV	Zero Emissions Vehicle

Definitions/Abbreviations

10%to90%BurnDuration	Burn Duration
50%MB	Combustion Phasing
AFR / λ	Relative Air-Fuel Ratio
ATDC	After Top Dead Centre
ATDCf	After Top Dead Centre firing
ATDCg	After Top Dead Centre gas exchange
BEV	Battery Electric Vehicle
BTDC	Before Top Dead Centre
BTDCf	Before Top Dead Centre firing
BTDCg	Before Top Dead Centre gas exchange
CAD	Crank Angle Degree
CO	Carbon Monoxide
CO_2	Carbon Dioxide
COV_{IMEP}	Coefficient of Variation of IMEP
DAQ	Data Acquisition
DI	Direct Injection
ECU	Electronic Control Unit
EGT	Exhaust Gas Temperature
FCEV	Fuel Cell Electric Vehicle
GHG	Greenhouse Gas
H_2	Hydrogen
HC	Hydrocarbons
ICE	Internal Combustion Engine
IMEP	Indicated Mean Effective Pressure
ITE	Indicated Thermal Efficiency
LNV	Lower Net Value
MVL	Maximum valve lift
NH_3	Ammonia
NOx	Nitrogen Oxides
O_2	Oxygen
PFI	Port Fuel Injection
PLC	Programmable Logic Controller
PM	Particulate Matter
PMEP	Peak Mean Effective Pressure
R_{max}	Pressure Rise Rate
SI	Spark Ignition
Sparkto10%BurnDuration	Crank angle of 10% mass burn

Appendix

Test cell measurement devices

Measurement	Device	Manufacturer	Measurement range	Linearity/Accuracy
Engine speed	AC Dynamometers (Asynchronous)	Sierra Cp Engineering	0-6000 rpm	±1 rpm
Engine torque	AC Dynamometers (Asynchronous)	Sierra Cp Engineering	-50-500 nm	±0.25% of FS
Clock Signal	EB582	Encoder Technology	0-25000 rpm	0.2 CAD
Hydrogen flowrate	Coriolis flowmeter K000000453	Alicate Scientific	0-10000 g/h	±0.20% of reading
Intake air mass flow rate	F-106 AI	Bronkhust	4-200 kg/h	±0.2% of reading
In-cylinder pressure	Piezoelectric pressure sensor Type 6125C	Kistler	0-30 MPa	≤ ±0.4% of FS
Intake pressure	Piezoresistive pressure sensor Type 4049A	Kistler	0-1 MPa	≤ ±0.5% of FS
exhaust pressure	Piezoresistive pressure sensor Type 4049B	Kistler	0-1 MPa	≤ ±0.5% of FS
Oil pressure	PX309-10KGI	omega	0-0.8 MPa	< ±0.2% of FS
Temperature	Thermocouple K Type	RS	233-1473 K	≤ ±2.5 K
Fuel injector current signal	Current probe PR30	LEM	0-20 A	±2 mA
PM emissions	DMS 500	Cambustion	0-5000 PPS	-
CO emissions	MEXA-584L	Horiba	0-12 vol%	≤ ±1.0% of FS or ±2.0% of readings
CO_2 emissions	MEXA-584L	Horiba	0-20 vol%	≤ ±1.0% of FS or ±2.0% of readings
O2	MEXA-584L	Horiba	0-25 vol%	≤ ±1.0% of FS or ±2.0% of readings
THC emissions	Rotork Analysis Model 523	Signal	0-5000 ppm	≤ ±1.0% of FS or ±2.0% of readings
NO/NO2 emissions	CLD 150 (Heated Chemiluminescence Detector)	Cambustion	0-500 ppm or 0-10k ppm	≤ ±1.0% of FS or ±2.0% of readings
H2 slip emissions	Air sens500	V&F	0-5000 ppm or 0-100% vol	0.5% of fs or 1%vol